ISTITUTO NAZIONALE DI FISICA NUCLEARE

Sezione di Catania

INFN/TC-93/07
14 Giugno 1993

A. Badalà, R. Barbera, F. Librizzi, D. Nicotra, A. Palmeri, G. S. Pappalardo,
L. Platania, C. Rapicavoli, F. Riggi, A. C. Russo, M. Salemi, A. Santoro, R. Turrisi,
A. Anzalone, L. Calabretta:

THE "CLAMSUD" MAGNETIC SPECTROMETER AS A PION DETECTOR

Servizio Documentazione
dei Laboratori Nazionali di Frascati

INFN – Istituto Nazionale di Fisica Nucleare
Sezione di Catania

INFN/TC–93/07
14 Giugno 1993

The "CLAMSUD" magnetic spectrometer as a pion detector

A. Badalá, R. Barbera, F. Librizzi, D. Nicotra, A. Palmeri, G.S. Pappalardo, L. Platania, C. Rapicavoli, F. Riggi, A.C. Russo, M. Salemi, A. Santoro, R. Turrisi

Istituto Nazionale di Fisica Nucleare, Sezione di Catania, Corso Italia 57, I-95129 Catania, Italy

A. Anzalone and L. Calabretta

Istituto Nazionale di Fisica Nucleare, Laboratorio Nazionale del Sud, V.le A. Doria, Catania, Italy

Abstract. - *The "CLAMSUD" magnetic spectrometer is described from the point of view of its optical properties and technical performances as a pion detector. Details on the focal plane detectors, as well as on the technical facilities are given. The results of a preliminar test are also reported.*

1. - Introduction

During the last few years, a large amount of experimental work was devoted to the study of pion production at beam energies below the free nucleon-nucleon threshold.

A first generation of experiments was concerned with inclusive measurements [1,2]. Unfortunately, different models based on various reaction mechanisms lead to the same values of inclusive observables, such as energy spectra and excitation function.

Recently, some semi-exclusive experiments have been performed in which charged pions were detected in coincidence with fission fragments [3] and light charged particles [4,5]. All the results of these experiments claim for the central character of the collisions producing pions. In ref. [5] the experimental data were successfully compared with the results of a theoretical model [6] for medium energy heavy ion reactions in the frame of a participant-spectator picture. In a recent work [7] the inclusive data contained in ref. [6] were also analyzed through a microscopic model, based on the numerical solution of the Boltzmann-Nordheim-Vlasov equation [8]. Both models give a reasonable agreement with the data and it is not yet clear if there is compatibility in the involved time scales. Then, the subthreshold pion production is still an intriguing problem. To sum up, further experimental and theoretical efforts are needed to draw a final answer on the subthreshold pion production mechanism.

On the experimental side, the most part of inclusive and semi-exclusive experiments on charged pion production were performed by means of a plastic scintillator range telescope [9]. Only few inclusive measurements were carried out by means of magnetic spectrometers [10,11]. In these experiments pions were detected at 0^0 only.

Even though a range telescope, like those used in the quoted experiments, is very

easy to handle and has a large solid angle ($\simeq 40\ msr$), yet it has many drawbacks:

i) its energy resolution is only about 3 MeV;

ii) because of the large ratio between contaminant protons and pions at low pion energies and forward angles, the threshold energy for pion detection ranges from about 30 MeV at backward angles to about 50 MeV at forward angles. Hence, it is hard to operate at angles $\leq 40^0$. The separation between pions and contaminant electrons is however not very critical, even at low energies where the ratio between electrons and pions is about 10;

iii) the efficiency for π^+ identification against π^- of $(80 \pm 2)\%$ is not adequate for a reliable deduction of π^+/π^- ratios;

iv) the corrections for the interactions of pions with the telescope materials are very strong expecially for high pion kinetic energies ($\simeq 40\%$ for 100 MeV pions).

It is evident that a magnetic spectrometer would eliminate the above stated drawbacks. On the other hand, coincidence experiments, performed with low duty cycle beams, need a high solid angle for π detection in order to reduce spurious coincidences to reasonable rates, without a drastic reduction of the pion counting rate. For the same reason it should be desirable to have a high momentum acceptance of the spectrometer.

Another interesting aspect in pion production is the pionic fusion, that can be schematized as follow:

$$A + B \longrightarrow \pi + C^*$$

where the fusion of the two nuclei A and B takes place, while part of the available energy is spent to produce a pion. So, in the final state there are only two bodies: the excited nucleus C and one pion. The pion energy spectrum reflects the levels of the compound nucleus, that very often is exotic (for instance $^{12}C(^3He, \pi^-)^{15}F^*$).

This kind of reaction is very interesting because the pion is produced in a reaction where a fully coherence takes place in the nucleus-nucleus (or nucleon-nucleus) interaction.

Up to now, only few measurements were performed on pionic fusion, since the corresponding cross-sections are very low. Two of them were performed by means of the QQD magnetic spectrometer *MATHUSALEM* ($\Delta P/P = 2.5\%$ and $\Delta\Omega = 6.2\ msr$) $^3He(^3He,\pi^+)^6Li$ at 282 MeV [12], $^4He(^3He,\pi^+)^7Li$ at 280.5 MeV [13], another one employing the spectrometer *OMICRON* ($\Delta P/P = 11.2\%$ and $\Delta\Omega = 5.5\ msr$) $^6Li(^{12}C,\pi^-)^{18}Ne$ at 86 MeV/u [11]. For this last reaction, only an estimate of 1 pb/sr as the upper limit for the $d\sigma/d\Omega$ for the first 11 MeV of excitation energy of the ^{18}Ne was given.

For this kind of measurements we need an instrument having the following characteristics:

1) A good momentum resolution

2) An high momentum acceptance

3) A large solid angle

4) Compactness.

The characteristic 1) is useful to resolve the different nuclear levels of the residual nucleus; the 2) and 3) are very important, since the cross-section to be measured is very low; the 4) is due to the fact that charged pions decay with a mean life at rest of 26 ns and then the path from the target to the focal plane detectors must be not very long in order to correct as low as possible the measured cross-section for in-flight decay.

Taking into account the above mentioned considerations, a magnetic spectrometer, named "CLAMSUD" [14], was built and installed at the "Laboratorio Nazionale del Sud" in Catania.

The main purpose of the CLAMSUD spectrometer is the detection of charged pions up to 240 MeV/c. The main characteristics of this magnetic spectrometer are:

i) the high solid angle ($\Delta\Omega \simeq 30msr$);

ii) The high momentum acceptance ($\Delta P/P \simeq 20\%$);

iii) the good momentum resolution ($\simeq 0.2\%$).

The present report is concerned with general performances of the CLAMSUD spectrometer, whose main characteristics are resumed in Table I.

The optical properties and the overall performances of the whole instrument (magnetic part and detectors) are obtained by simulation by means of the code GEANT2 [15]. The description of the numerical simulation is outlined in Sect. 2.

Sect. 3 is devoted to the general description of the spectrometer (geometry and magnetic field). The optical properties of CLAMSUD are described in sect. 4. The focal plane detectors are described in sect. 5. Sect. 6 is devoted to the study of contaminants. Some study of the CLAMSUD performances depending on the employed beam sizes is shown in sect. 7. The NIM electronics and acquisition system are described in sects. 8 and 9 respectively. Sect. 10 is devoted to the description and results of some specific experimental tests. The main facilities of the spectrometer are described in sect. 11. The conclusions are drawing in sect 12. In the appendix the main optical characteristics are derived in the case of a source position far from the optimal one.

2. - General description of the numerical simulation

Before speaking about the numerical simulation it is necessary to anticipate that the apparatus to be simulated is constituted essentially by the CLAMSUD dipole and the focal plane detectors. These are given by two wire chambers and two planes of plastic scintillators (see sect. 5).

To simulate the physics of the spectrometer, the program GEANT2 [15] was employed in tandem with a data reduction code. This philosophy allowed us to analyze the simulation results also in an event by event basis. In particular, the GEANT2 program, that incluses the geometry of the spectrometer and the associated focal plane detectors, is used to generate a set of simulated events. Each event is made of 9 *words* (2 byte each): a *flag* that gives the kind of particle hitting the two wire chambers (for instance pion or muon), the two coordinates of the intersection of the particle with the first wire chamber, the two coordinates relatives to the second wire chamber, the energy loss in each scintillator plane and the two time of flight of the particles from the source to each plane of scintillators. Afterwards the file of events is read by the data reduction code, that builds as many spectra we want. In the read-out of the simulated events, all the usual features of a data analysis program can be used, including definition of virtual words (calculated from the original ones), one- and two-dimensional contours, any combination of logical conditions ...

Another advantage on the above-stated philosophy is due to the speed of the data reduction code, that allows us to quickly remake the analysis from a different point of view employing the same event file, if the general characteristics of the simulation are not changed.

All presented calculations were performed by means of a *Digital VAXstation 3100/M38*. The CPU time needed to generate an event by the code GEANT2 is about 1.3 seconds. This means a CPU time of about 36 hours for 10^5 events. On the contrary, the corresponding CPU time to process 10^5 events by the data reduction code is less than one minute. So, in order to obtain results with a better statistics it would be preferable to employ a more powerful computer.

3. - General description of the spectrometer

3.1 - Geometry

The CLAMSUD spectrometer layout is presented in fig. 1a. It consists of a bending magnet with non-parallel poles. This solution was firstly proposed by H. Enge and S. Kowalsky [16] for the CLAMSHELL spectrometer installed at Los Alamos.

The spectrometer will be operated mainly with heavy ions beams and at 0^0, so a big window to bring out the primary beam was created inside the return yoke of the magnet. Moreover, this aperture offers the opportunity to place detectors inside the dipole for coincidence measurements. The dipole is placed on a rotating support and its bending plane is vertical. When placed at 0^0, the dipole accepts particles emitted in $\pm 4^0$ along the reaction plane. Moving the spectrometer closer or farther near the target point (35÷100 cm) it is possible to measure the angular distribution in the angular range $25^0 \div 140^0$. CLAMSUD, as CLAMSHELL, is a compact spectrometer; so, the trajectory lengths are very short and the in-flight decay of the pions between the target and the detectors is then minimized. The main characteristics of the dipole are presented in Table I.

In fig. 1b it is shown the spectrometer as described in the code GEANT2. The axial position of the poles is also described inside the code, so each particle that hits the pole or goes out of the spectrometer is considered lost. The "master" system has its origin at the entrance point of the central trajectory; the X_M-axis is along the field generatrix (i.e. the straight line where the field has a constant value of B_0) and is oriented as in figure; the Z_M-axis is perpendicular to X_M; the Y_M-axis is perpendicular to the median plane and is oriented to form with the other axes a clock-wise system. Two other coordinate systems are also shown in fig. 1b: the source system (suffix S) and the focal plane system (suffix F). These last two systems have the Y-axes parallel to Y_M. The chosen coordinate systems are taken according to the standards of the code "RAYTRACE" [16], which was employed to design the

spectrometer and to test the results of GEANT2.

3.2 - Magnetic field

Since the poles of the magnet are not parallel, the magnetic field is not constant and its behaviour generates an axial focusing force, along the particle trajectory, that increases the angular acceptance of the magnet.

The magnetic field of the spectrometer can be divided into three regions: a) entrance fringing field region, b) field gradient region, c) exit fringing field region.

In the field gradient region the magnetic field components in the median plane are:

$$B_x = B_z = 0$$

$$B_y = B_0(1 + \frac{1}{B_0}\frac{dB}{dr}\Delta r) = B_0(1 + n\Delta r/R) \qquad (1)$$

where R and n, respectively curvature radius and field index of a magnet, are introduced only for reason of uniformity of description with RAYTRACE code and the standard way to describe the bending magnet. In fact the field changes according to (1) along the perpendicular to the generatrix of the pole, (see fig. 1b), being constant along the line parallel to the generatrix. The value of R and n respectively of 8500 cm and 70 were chosen to fit the experimental gradient.

Δr is the distance of the point (x,z,y) from the generatrix (X-axis).

The field values outside the median plane are evaluated by the well know law *curl* B= 0. Practically the same formula used in RAYTRACE program was installed in the code GEANT2.

In the fringing field regions and for magnets with a constant gap and straight boundary, the field is generally described by the following formula:

$$B(z) = B_0/(1 + e^{C_0+C_1(s/d)+C_2(s/d)^2+C_3(s/d)^3+\cdots}) \qquad (2)$$

where s is the distance from the boundary and d is the gap of the magnet. In our case the gap along the entrance boundary is variable, the EFB (effective fringing boundary) is curved and tilted by 34.8^0 with respect to the entrance trajectory. The evaluation of the magnetic field takes into account this shape by summing up with different weights the contributions evaluated by (2) due to different pieces of poles. We employed for the calculations the same technique proposed in the RAYTRACE code to which we refer the reader. The employed C coefficients (see ref. [16]) for the description of the entrance and exit fringing field were deduced by magnetic field measurements.

A grid of magnetic field was measured by means of a Hall probe at entrance and exit sides with 1 *cm* steps. Data were measured along 5 lines parallel to the entrance direction separated by 1 cm. Similarly for the exit side the data were measured along 7 line parallel to the exit direction, separated by 5 cm.

To study the spectrometer by simulation we need mainly the position of the EFB and the C_i parameters that describe the magnetic field shape at the entrance and exit sides. These parameters were extracted from the experimental data. For the C_i the following iterative fitting procedure was used.

i) The coefficients are first obtained fitting the experimental data to eq. (2);

ii) these coefficients are used in the RAYTRACE program to evaluate the field along the experimental line;

iii) differences between the experimental data and the simulated ones were used to modulate the original experimental data and this new data used in a new fit-

ting run. After 5-6 iterations a good agreement between the original experimental data and the field computed by RAYTRACE was obtained. These C_i coefficients, parameters describing the entrance and exit EFB position and orientation, and the experimental gradient measured perpendicular to the generatrix were put inside the RAYTRACE and GEANT2 codes to evaluate the characteristics of the spectrometer.

4. - Optical properties

4.1 - Focal plane determination

The position of the focal plane and its extension depend obviously on all the parameters describing the spectrometer. The study was performed varying only the parameters that can be still modified in the course of the installation stage, in particular the source location.

In order to investigate the effects of these parameters, we evaluated by means of the code GEANT2 the focal plane position, the particle images on the focal plane and the spectrometer solid angle.

The location of the focal plane was determined assuming to transport stable particles that enter into the spectrometer through a fixed collimator. By means of the code GEANT2, the intersections of the trajectories with two convenient planes are calculated for a given value of the linear momentum P of the particle. The first extracted trajectory is always the central one, (*i.e.*, the first particle is emitted at $\theta = 0^0$ in the source frame), while the other ones are randomly extracted in a given solid angle $\Delta\Omega$ around the Z-axis of the source frame. The source frame has the origin on the source (suffix S in fig. 1b). The two planes are chosen far enough from the exit side of the magnet, where the particle trajectories are surely straight lines. The obtained values of these couples of coordinates are recorded in a file. Afterwards, another program evaluates the trajectory equations (*i.e.*, the straight

lines intercepting each of the couples of coordinates). Then the coordinates of the intersections of the various trajectories with the central one are evaluated. Finally the centroid of such coordinates is evaluated. It represents a point in the focal plane corresponding to the given linear momentum P.

The above calculations are repeated for various P values around the central momentum P_0.

As an example, for a central momentum $P_0 = 200\ MeV/c$, the calculations were performed from $P = 150\ MeV/c$ up to $P = 270\ MeV/c$ with 10 MeV/c steps. The number of random extractions for each P value was 100. In the calculations of centroids, values deviating more than 3 standard deviations (*s.d.*) from the mean value were rejected. The points corresponding to linear momenta from 160 to 240 MeV/c ($\Delta P = 20\%$) lie effectively on a plane, as it results from the correlation coefficient $r = 0.9993$ of the linear regression obtained taking into account only these last points.

The above exposed example is synthesized in Table II (see captions); the resulting focal plane equation in the master system is $z = 0.23x + 12.07$. The central trajectory crosses the focal plane at $(X_0,\ Z_0) \equiv (96.75,\ 33.97)$ (The units are *cm*).

In this example and in all other calculations presented in the following the source was placed at a distance of 35.5 *cm* from the entrance of the magnet and the source system was rotated by $\theta_s = 25^0$ with respect to the master. The entrance collimator angle is 100 *mrad* along the X-axis and 75 *mrad* along the Y-axis in the source frame.

4.2 - Other optical properties

In order to investigate if the CLAMSUD characteristics, such as solid angle and momentum resolution, can be improved, we performed different estimations of the

focal plane position and related characteristics by moving the source position from an original point (S_0 in fig. 1b). We moved the source position by 1 *cm* steps along the perpendicular to the line intercepting the original position and the origin of the master system. The displacement Δx was performed along the direction approaching the focal plane (left side in fig. 1b). The results of this investigation are presented in Table III and in fig. 2. It is evident that the best case is obtained with a source displacement Δx of 2 *cm*, where the momentum resolution reaches the value of $2.63 \cdot 10^{-3}$ (against $3.53 \cdot 10^{-3}$ at the original source position) while the solid angle is only slightly decreased. In the best case the focal plane is slightly shifted by about 1.5 *cm* towards the exit of the magnet with respect to the original case.

All the above mentioned calculations were performed putting a collimator at the entrance of the magnet that accepts particles emitted ± 75 *mrad* axially and ± 100 *mrad* radially. We have investigated if it is reasonable to increase the aperture of the entrance collimator. It is evident that we do not gain in the axial direction, because of the particle hit on the poles. The investigation was then performed increasing the radial collimation. The results are presented in Table IV. As expected there is an increase of the solid angle but a deterioration of the momentum resolution. The conclusion is that we have the possibility to choice the appropriate collimation according to the experiment requirements; for instance if we do not need a good momentum resolution (as it is the case in continuum spectra measurements) we can employ a large collimator with a net gain in statistics for a given run time.

Another improvement can be obtained on $\Delta P/P$ linear momentum acceptance. In fact, for a given field it is possible to extend measurements to $\pm 20\%$, as shown in Table V with a slight decrease of the solid angle at the two extreme momenta. In this case the dimensions of the focal plane detectors need to be increased, since the radial length of the focal plane becomes 46.3 *cm* instead of 36.0 *cm* for a $\Delta P/P = \pm 15\%$.

Typical particle images on the focal plane for the three linear momenta P_0, $P_0 - 15\%$ and $P_0 + 15\%$ are shown in fig. 3a. A magnified image corresponding to the central momentum is also shown with a better resolution in fig. 3b.

The "banana shape" of the image indicates that for a given bin of Z_F values, the resolution is better than that obtained from the projection of the whole image on the X_F axis. This is possible measuring the axial position on the focal plane. The obtained improved resolutions are reported in Table VI for some bins of Z_F.

5. - Focal plane detectors

The determination of the particle hit on the focal plane of a magnetic dipole is of course essential in order to know its linear momentum. In order to reconstruct the particle trajectory, it is also important to know the angle of incidence of the particle on the focal plane. As we shall see in sect. 5.3, the knowledge of such an angle is very useful also to eliminate a large amount of muons that contaminate pion spectra. Therefore it is necessary to have two position detectors in order to determine the trajectories of particles emerging from the spectrometer.

In order to discriminate among different particles having the same linear momentum, it is important to measure their energy loss. The effective surface of the focal plane being of the order of 1600 cm^2 and the energy resolution of the energy loss being not crucial, it is a good choice to employ sets of plastic scintillators.

For what stated above, the detectors that were chosen to be installed close to the focal plane are: a) two multiwire chambers (MW1 and MW2), whose characteristics are described in sect. 5.1; b) two sets of 0.2 cm thick plastic scintillators (SC1 and SC2), described in details in sect 5.2

The mutual distance between the detectors is fixed in all reported calculations. Only the relative location of the focal plane frame with respect to the master changes

with the parameters.

In fig. 1b the detector planes are sketched in the frame of the focal plane. The distances of the detector planes from the focal plane are 20, 30, 40 and 60 *cm* for MW1, MW2, SC1 and SC2 respectively.

In order to estimate the useful dimensions of the detector planes, the image of the particles on the four planes where the detectors lie is evaluated for values of $P = P_0$ and $P = P_0 \pm \Delta P$ ($\Delta P = 15\% P_0$). Moreover the image on the focal plane is also evaluated digitizing with a given precision (for instance 1 *mm*) the hit of the particles on the two MW and hence reconstructing the hit with the focal plane. In this way it is possible to compare the true image with the recalculated one on the focal plane.

The resulting useful dimensions of the detectors are: MW1 ($52 \cdot 22$ cm^2), MW2 ($61 \cdot 24$ cm^2), SC1 ($69 \cdot 27$ cm^2) and SC2 ($85 \cdot 32$ cm^2) where the first number in parenthesis is referred to the radial dimension and the second one to the axial dimension.

5.1 - Drift chambers

The main parameters of the two drift chambers [17] are collected in Table VII. They consist of one anode plane and two cathode planes.

The anode plane is made by 50 μm Cu-Be wires, called *anode wires* or *sense wires*, and alternatively by 100 μm wires, called *potential wires* or *field wires*. The role of the latter is to help the electron collection on the sense wires. Usually it is useful to idealize a drift chamber as an assembly of contiguous cells; each cell has at its center a sense wire and at the extremities the potential wires.

The distance between the *sense* and *potential* wires is 4 *mm*. These wires run along the short side of the chambers.

The cathodes planes are made of 100 μm wires, running along the long side of the chambers with a spacing of 2 mm. The gap to the anode plane in between these cathode planes is 8 mm.

Two kapton foils separate the gas volume from the atmosphere. On the inner sides these foils are aluminized and the aluminium layer is kept to ground potential.

The typical drift-time is 20 ns/mm and then the drift time is in the interval $0 \div 80$ ns and is almost linear with the distance from the anode wire.

The high voltage is supplied to the cathode planes and the potential wires; the anode wires are kept to ground via the amplifiers.

The drift chambers operate in the self-quenching streamer mode [18]. So, the typical signals on the anodes are of the order of 200 mV and hence a low gain amplifier is needed. The recommended gas mixture to reach this mode is: $\sim$ 45% argon, $\sim$ 50% iso-butane and $\sim$ 5% heptane.

The horizontal coordinate is determined by measuring the drift-time of the electrons to the nearest anode wire. The wire chambers are positioned parallel to the focal plane, so the angles between the trajectories and the anode plane are in the interval $35° \div 63°$. This assured us that each trajectory intercepts more than one cell and then it is possible to resolve the left-right ambiguity, that is often considered as a drawback for drift chambers.

Each anode is connected to an amplifier-discriminator. The electronic modules, with eight channels per card, are directly mounted on the chambers. The ECL output signals are transferred via twisted cables to the TDC modules. All cards on one chamber have a common threshold input.

The vertical coordinate is determined via delay-line readout of the induced pulses on one of the cathode planes. The wires are connected in groups of three wires and each group is connected to the high voltage via a 1 $M\Omega$ resistor, and on the other

hand, via a 220 pF capacitor to a delay line. At both ends of the delay line, directly on the chamber, two amplifiers are installed. These signals are then fed to a constant fraction discriminator.

There are four independent power supplies [17] for cathodes and potential wires for the two chambers. The maximum output is -3kV for the potential wires and -5kV for the cathode planes. In case of over current (adjustable between 0.5 and 30 μA) the HV output is lowered in steps of 75% of the initial value until the current falls below the current threshold; after some minutes, the current reach again the set value.

The gas flux and the relative percentages of the mixed components are electronically controlled by a mixing gas station. The *iso-butane* and *argon* bottles are connected each ones to a mass-flow-meter. The electronic control unit is connected with the two flow-meters and determines the gas flow of the two gases. In particular, operating with an elipot and looking at a display, it is possible to fix the total flux and the percentage of *argon* with respect to *iso-butane*. The gas *argon*, coming out from its flow-meter, enters into the inlet of the gas-washing bottle, filled with *heptane*. From this bottle an *argon-heptane gas-mixture* comes out. It results that a quantity of *heptane* vapor is added to the *argon* gas; according to the Dalton law this quantity results to be about 10% of the *argon*. Finally, the *iso-butane* and the *argon-heptane* mixture are mixed together and are sent via two gas flow meters to the two chambers.

5.2 - Plastic scintillators planes

The two scintillators planes are made of plastic scintillators 2 mm and 4 mm thick for the first and the second plane respectively. Each scintillator has a rectangular form, with the longest side along the axial direction and the shortest side

along the radial one. The longest side dimension was chosen in order to largely cover all the axial useful length: $35cm$ for the scintillators of the first plane and $40cm$ for that of the second plane. We chose the scintillator dimensions along the radial direction, taking into account some results of the simulation code. We found that an optimal length is 8 cm. In fact, within this choice, it is easy to see, by means of the simulation, that, if one scintillator of the first plane is fired, not more than three given scintillators of the second plane can be fired, taking into account the realistic trajectories of stable particles. On the right side of fig. 4 this correspondence is shown, where "i" and "j" indexes are referred to the order number of scintillators on the first and second plane respectively.

6. - Simulation study of contaminants

6.1 - Electrons and protons selected by the CLAMSUD $B\rho$

Pions detected by means of a magnetic spectrometer are to be discriminated among the other particles having the same linear momentum. A very simple possibility is to perform an energy loss - time of flight analysis.

Various $\Delta E - t$ scatter plots are shown in figs. 5 through 7.

Pion-proton discrimination is shown in fig. 5 for $P = 200\ MeV/c \pm 15\%$ (corresponding to 104.3 MeV pion energy and 21.1 MeV proton energy). It is evident that a simple cut on the time of flight is able to separate the two particles. For smaller linear momenta the time separation is obviously better.

The pion-electron separation is shown in fig. 6 for $P = 50\ MeV/c \pm 15\%$.

For sake of completeness we also calculated the scatter plot around $P = 200\ MeV/c$, shown in fig. 7. No direct observation has been performed for such high energy electrons at beam energies around 100 $MeV/nucleon$. However, a recent theoretical work [19], concerning the dilepton production, evaluates the pion

production cross section about 2 orders of magnitude greater than the dilepton one.

As shown in fig. 7 a cut on the time of flight is not sufficient, but for $P = 170\ MeV$ it is still possible to discriminate by putting limits in the $\Delta E - t$ plane.

6.2 - Protons coming from the source, not selected by the $B\rho$ of the spectrometer

In order to reject from the trigger the particles coming from the source, but not passing through the dipole (*i.e.* the particles not selected by the the $B\rho$ of the dipole), it is suitable to put in front of the entrance of the spectrometer one or two very thin scintillators. The signal coming from these scintillators have to be put in coincidence with that coming from a suitable coincidence of the two scintillator planes. Details on this coincidences are shown in Sect 8. Any case, if the above mentioned *input* scintillators are not present, it will be very difficult to mix together pions selected by the dipole with protons from 20 to 600 MeV, coming directly from the source, as it is clearly evidenced in fig. 8. In fact, even if there is a superposition in time, a clear separation in energy loss takes place.

6.3 - Muonic contamination

Since pion is not a stable particle, the number N_π of pions that hit the detector is given by:

$$N_\pi(t) = N_0 \cdot exp(-t/\tau) \qquad (1)$$

where N_0 is the number of pions emitted by the source (taking also into account the corrections due to the magnet solid angle), t is the time of flight from the source to the detector and τ is the pion mean life in the *lab* frame.

$$\tau = \tau_0 \cdot (E/m) \tag{2}$$

$\tau_0 = 26.03\ ns$ is the mean life of the pion at rest, E is the total energy of the pion and m its mass.

Hence, the number of pions effectively emitted by the source is:

$$N = N_\pi(t) \cdot \epsilon_s \cdot \epsilon_d \tag{3}$$

where

$$\epsilon_s = \Delta\omega/4\pi \tag{4}$$

is the efficiency factor taking into account the solid angle and

$$\epsilon_d = \frac{1}{exp - [(t \cdot m)/(\tau_0 \cdot E)]} \tag{5}$$

is the efficiency factor taking into account the loss of pions due to the in-flight decay.

Unfortunately, the problems due to the in-flight decay cannot be resolved simply by applying the eq.(3), since a given number of μ, emitted in flight by the pions can reach the focal plane detectors and a part of them is not distinguishable from pions. Hence, it is important to evaluate the percentage of contaminant μ by the simulation program.

The input pion spectrum, extracted within the GEANT code, is a realistic one: it is assumed equal to the π^- spectrum measured in the reaction $^{58}Ni(p,\pi^-)X$ extrapolated up to zero MeV. The calculation was repeated for four values of the

magnetic field B_0, corresponding to the values $P_0 = 50,\ 67,\ 90$ and $120\ MeV/c$ of the linear momentum of the central trajectory.

The image of particles reaching the first wire chamber is given in fig. 9a and 9b (the horizontal and vertical axes give the radial and axial direction respectively). Fig. 9a is referred to pions as well as muons, fig. 9b only to pions. On fig. 9b the contours that include strictly the image were taken. The polygonal vertex of this contour were memorized on a file and subsequently utilized as conditions to reject muons. A similar procedure was done for the image of particles reaching the second wire chamber (see fig. 10a and 10b).

The matrix θ_x, θ_y, where the axes represent the angles between the particle trajectory and the focal plane along the radial and axial direction respectively, is represented in fig. 11a and 11b. Fig. 11a is referred to pions and muons, fig. 11b only to pions. In the case of only pions (fig. 11b) the boundaries are very clear and then it is possible to take the contours on this matrix for a further utilization.

The momentum spectra are obtained from simulation with the condition of the *flag* value for pions, or with the above-stated conditions that reduce the muon number without affecting the pion number. In Table VIII (see caption) the percentage rate of contaminant muons is shown in the case of no condition applied and when the aforesaid conditions are applied.

As shown in Table VIII the applied conditions strongly reduce the μ contaminant number that at most reaches 3%.

Fig. 12 shows the obtained spectrum (squares) of pions plus residual contaminant muons that still remain after the application of the aforesaid conditions. This spectrum results to be indistinguishable from that obtained without the contaminant muons (not presented), since the muon contamination results less then the statistical errors. The simulated spectrum (squares) is compared to the starting one

(histogram) after correction for the CLAMSUD solid angle and for the in-flight decay of pions. This last correction depends from the applied magnetic field and from the particle momentum (for a given magnetic field it is possible to establish a biunique correspondence between the particle momentum and an average time of flight of the particle; so it is possible to evaluate the ϵ_d correction, given by the relation (4)). The threshold, visible in fig. 12 for the simulated spectrum, is due to pions of energy less then $\sim 8.5\ MeV$ that are stopped in the first scintillator plane and so cannot reach the second one.

An analogous simulation procedure is also made for another assumed spectrum, that presents some discrete peaks (it was assumed as starting spectrum the measured pion spectrum from the reaction $p + {}^{12}C \longrightarrow \pi^+ + {}^{13}C^*$ obtained with 201 MeV protons). The results of such a simulation are presented in fig. 13.

7. - Simulation study with different beam sizes

The simulation study presented in sect. 4.2 was performed in order to extract the intrinsic optical properties of the CLAMSUD spectrometer. Consequently, these properties were extracted taking into account a size-less source. This is not the case in real experiments, where the profile of the beams impinging on the target have a finite size.

In order to study the momentum resolution of the apparatus as a function of the source size, we introduced in the simulation code a vertex position that can change randomly inside a cylinder centered on the old source position. The thickness of the cylinder is chosen 20 μm, taking into account a typical target thickness.

We found that from 0 up to 10 mm of diameter for the source size, the resolution is not affected. The resolution is about $5 \cdot 10^{-3}$ for a diameter of 50 mm.

Fig. 14a, b and c show qualitatively the effect of the source size on the resolution

for a diameter d=5, 40 and 80 *mm*. The input spectrum is the same shown in fig. 13 for a size-less source.

8. - NIM electronics

The electronic scheme to create the trigger is shown in fig. 4.

The analogical signals coming from the photomultipliers (PM) associated to scintillators, are firstly connected to "linear FAN OUT" (lin F.I.O). PM A indicates the photomultiplier associated to the start scintillator, placed at the entrance of the dipole. PM B_i and PM C_j indicate the photomultipliers associated to the first and the second plane of plastic scintillators (9 and 11 respectively). One output of the "linear FAN OUT" is connected, through a suitable delay line, to a charge converter (ADC); another output is connected to a constant fraction discriminator (dis FCC8). The employed c. f. discriminator (the FCC8 by GANELEC) is a CAMAC module and can be controlled by computer; it gives output in the ECL standard; we need to convert the output signals into NIM, by means of a conversion module (ECL-NIM). One of these is employed to send signals to the starts of a TDC.

As explained in sect. 5.2, it is shown by simulation that if one scintillator of the first plane is fired, not more than 3 consecutive scintillators of the second plane can be fired in the same event. So, it is useful to take advantage of this optical property to better define the "trigger". So, following the table shown on the right side of the figure, the logic "OR" of the scintillators (1,2), (2,3), (3,4,5) etc... of the second plane is performed by means of a "logic FAN IN" (logic F.I.O.). Successively, the suitable coincidences between the signals coming from the first plane scintillators and the corresponding mixing of the second plane scintillators are performed following the correspondence table. Of corse, a suitable fixed delay line (R) is needed, as shown in figure. All the obtained coincidences are then mixed by a logic "OR" (logic F.I.O.).

The obtained signal is finally put in coincidence with the signal coming from the "start scintillator A". The logical signal coming from the start scintillator goes to the coincidence (COIN) through a variable delay line. The signal width and the delay are tuned in order to have only coincidences between signals originating from pions. This is possible due to the very good separation in time between pions and protons selected by the same $B\rho$ interval. Of corse, there is a proper delay for each selected B_0 of the dipole.

On the lower side of the figure a standard LAM (look at me) signal for the acquisition is shown: the trigger signal is split by means of a logical fan-out (logic F.I.O.). One output goes to the common stop of a TDC; another one goes through a gate generator (G.G.) to the GATE input of the ADC; another one goes to a logical module (for instance a discriminator), that gives the signal to be sent as LAM. The LAM signal can be vetoed by a *veto* signal. This *veto* signal is a mixing of the *veto* coming from the acquisition and a signal coming also from the trigger, delayed and having a duration of about $100\mu s$. Other signals can be mixed to the *veto*-mixer; for instance a signal coming from the wire chamber power supply, that is sent whenever the set high voltage goes down.

9. - Acquisition system

Standard electronics was used for the acquisition, which includes CAMAC ADC and TCD.

For the drift chambers, part of the LeCroy Mod.4290 System is used. This is a complete operating system for multiwire drift chamber data acquisition. It consists of time digitizers modules, control/read-out units and interface buffers. The 4291 TDC modules are placed in a dedicated standard CAMAC crate. The inputs to the TDC are provided by ECL signals which are generated by the amplifier/discriminator/ECL

drivers cards directly mounted on the chamber. A drift chamber TDC controller, Mod.LeCroy 4298, is placed in slots 24 and 25 of the dedicated crate. This crate controller performs fast data read-out, rejecting zeros and full scale values during data taking. Valid data are dumped via a fast bidirectional databus into a parallel access, 4K x 16 bit memory, located in a standard CAMAC crate, together with other CAMAC modules. These include a set of ADC and TDC units and a trigger unit.

The use of the CLAMSUD spectrometer requires a dedicated acquisition system to carry out all the necessary calibrations procedures of the apparatus before it becomes fully operational and, at a later stage, for in-beam data taking. The usual tasks of a general acquisition system are required, namely the acquisition and storage of data, a check of the correct functioning of the detectors, and on-line analysis of some of the parameters being collected. Compatibility with similar systems and modular assembling are also useful features to be demanded.

For these reasons a system based on CAMAC + VME standards, coupled to a MacIntosh processor, was developed, similar to other systems presently in use at the *Laboratorio Nazionale del Sud.* Particular features which take into account the structure of the focal plane detector for the CLAMSUD spectrometer have been implemented in the present version of the system.

On the whole, around 180 TDC channels are provided by the drift-chambers, and about 40 ADC+TDC channels by the hodoscope and start detector.

All the software is written in Real Time Fortran (RTF) language. This allows to use global common blocks which can be addressed through the VME bus by different processors. Several programs are concurrently executed by the system: i) The readout program, running on the I/O processor; ii) one or more analysis programs, running on the corresponding analysis processors; iii) the control program

which runs on a MacIntosh computer.

The data which are read out by the I/O processor are allocated in the acquisition buffer and, through the same readout process, are transferred to the main buffer. Data are collected from this buffer by the analysis processor to build up spectra, which are allocated into the VME RAM Spectra Buffer. The control program reads spectra from this buffer for display and on-line analysis. This program is also used as a user interface, providing error messages, different menues, output of spectra,...

A variable record length is used to define the event structure; this includes a pattern word, which initiates the event, and a variable number of words coming from the CAMAC electronics.

The analysis program, running on its dedicated processor, handles the main buffer and the building of spectra. The main buffer is organized as a FIFO (First In First Out) memory, which is filled by the readout program. Readout of records from the FIFO can be executed concurrently by several processors. The access to the record is a multistep process (allocation of ENTRY, readout and transfer of the ENTRY, deallocation, deleting). The handling of large data structure and the routines for the building of the spectra have been extracted from the general package LISA (Low energy Interaction Spectra Analysis)

The control program, running on a MacIntosh II FX processor, is the main part of the acquisition system; it allows a decoding of the user commands and at the same time acts as a monitor of the status of the system, providing a user friendly interface to the system. This has been developed by using the software facilities MacSyS oriented to VME-MacIntosh acquisition systems. The main part of this facility include a RTF/68K compiler, a M68mil assembler, a linker, a graphic library (MiniGD3), an icon and window oriented package (ResEdit). For the display and analysis of the spectra, the control program makes use of the MiniGD3 package,

which allows to handle one and two dimensional spectra on several windows of the screen.

10. - Test measurements

The calculated optical characteristics of CLAMSUD were experimentally checked, employing a composite alpha radioactive source. The source was a miscellaneous of 241-Americium, 244-Curium and 239-Plutonium. It was placed on the CLAMSUD source position with a 1 *mm* collimator to limit its extension. A silicon position sensitive detector was placed on the calculated focal plane at its center. The dimension of the sensitive area was 4 *cm* along the radial direction and 1 *cm* along the axial one. In Fig. 15 two linear momentum spectra of the detected alpha particles are shown. The spectrum in Fig. 15b is measured with a magnetic field increased by a factor 1.03 with respect to the one in fig. 15a. The obtained resolution and dispersion are very close to the calculated ones.

11. - Descriptions of the main facilities

11.1 - Mechanics and movements of the rotating platform

The magnet is placed on a rotating platform. This last stands on a central pivot on one side and on a circular rail on the other side. Both the pivot and the rail (5 *m* of diameter) are well fixed on the ground. A stainless steel graduated strip is placed on the external side of the rail in order to read the angle, within a precision of 1 degree.

The platform stands on the rails through a pair of cone-shaped wheels. A translation platform is coupled to the rotating one by means of ball bushings and linear guides.

The rotation is made possible by a motor reducer. The self-braking motor (0.37 KW) is coupled directely to the conical crawler wheel, that by friction makes possible the rotation.

The traslation (up to 100 cm) occurs by means of an internal thread coupled to a crank by means of a reduction gear, arranged beforehand for an eventual motorization.

11.2 - CLAMSUD power supply and its remote control

The CLAMSUD spectrometer is equipped with a power supply, model S-8000, made by Danfisik which provides a continuous current up to 480 A with a time drift of less than ± 10 ppm. This magnet power supply can be local controlled and remote controlled via a RS-232 interface connected to the serial port of a personal computer. The control program running on the PC allows the user to switch on and off the power supply, to change the field polarity, and to set the desired value of the current (in percentage units of the maximum current). The computer is also connected by means of another serial port with a Hall probe unit which monitors the value of the magnetic field in a fixed position.

12. - Conclusions and outlook

In the present report the general description of the CLAMSUD spectrometer is presented. This description is based on simulations performed by means of the GEANT2 code coupled with a data reduction code. Details are given on the focal plane detectors that were realized, taking into account the results of the simulation code. Moreover some technical details are also given on focal plane detectors as well as on the other facilities of the spectrometer. The present report has the purpose to show the characteristics of the CLAMSUD spectrometer, but it can also be seen as

a technical description, even if it has not the pretension to be a complete "technical manual".

It is important to remark that the optical properties of the spectrometer, make also possible in principle its employment in fields of the nuclear physics different from the pion production. For instance it is possible to employ it for kaon detection or to detect low energy particles, coming from reactions in the TANDEM energy domain. Of course, in these cases it is necessary to design new focal plane detectors.

13. - Appendix

Focal plane and optical characteristics obtained with a source positioned at ~85 cm from the entrance boundaries

All calculations and considerations presented in this report are referred to a source placed at 35.5 cm from the entrance fringing boundaries. This source position corresponds practically to 4 *cm* outside from the entrance flange. It is possible to work with this source position in two cases: a) the spectrometer is placed at 0° with respect to the beam direction; b) one or two quadrupole lens are placed between the target and the magnet in order to focalize the particles to the given source position.

The possibility to introduce quadrupole lens is now under investigation. Some calculations are needed to decide on its employ. Any case, it is sure that, even if we gain in solid angle, we surely loss in the efficiency due to the in-flight decay, since we need a longer path of the particles. Moreover, if we employ only one quadrupole, distortions are expected on the focal plane, that will not be a real plane, but a surface.

Calculations performed with a source placed at 85 *cm* from the entrance fringing boundaries are presented in this section.

In these new conditions, the focal plane results to be about parallel to the one calculated with the standard source position, but it is about 10 *cm* more close to the output fringing boundaries.

The new calculated solid angle is 5.05 *msr*. The momentum resolution is $2.25 \cdot 10^{-3}$, very close to the standard one; the new dispersion (1.14 *cm*/%) is slightly smaller than the standard one.

It is possible to employ the same detectors designed for the standard case and placed about on the same positions, since their useful surfaces result to be smaller, due to the smaller dispersion.

In conclusion, the only drawback in putting the source 50 *cm* far from the standard position is the loss in solid angle.

9. - Acknowledgements

The authors are grateful to G. Lo Faro for his helpful contribution in building the mechanics to support the focal plane detectors. Many thanks to G. Barbagallo, C. Calì and F. Ferrera for their fundamental technical support and helpful suggestions on the acquisition system. G. Attinà and A. Maugeri are warmly acknowledged for their valuable support in CLAMSUD installation and alignment. The machine and electronic staff of the Laboratorio Nazionale del SUD are warmly acknowledged for their technical support.

References

[1] P. Braun-Munzinger and J. Stachel, Ann. Rev. Nucl. Part. Sci. **37** (1987) 97
and references therein
W. Benenson, Nucl. Phys. **A482** (1988) 503c

[2] E. Grosse *et al.*, Nucl. Phys. **A447** (1986) 611c
V. Bernard *et al.*, Nucl. Phys **A423** (1984) 511
G. Sannouillet *et al.*, Nuovo Cimento **A99** (1988) 875

[3] B. Erazmus *et al.*, Nucl. Phys. **A481** (1988) 821

[4] S. Aiello *et al.*, Europhysics Lett. **6** (1988) 25

[5] R. Barbera *et al.*, Nucl. Phys. **A518** (1990) 767

[6] A. Adorno *et al.*, Nucl. Phys. **A488** (1988) 451c

[7] A. Badalá *et al.*, Phys. Rev. **C43** (1991) 190

[8] G. Bertsch, S. Das Gupta, Phys. Rep. **160** (1988) 190 and references therein.

[9] J. Julien, Proc. 3rd Int. Conf. on Nuclear Rection Mechanisms
June 12-19 (1983) pag. 599 Varenna, Italy *see also:*
V. Bernard *et al.*, Nucl. Phys **A423** (1984) 511 *and*
G. Sannouillet *et al.*, Nuovo Cimento **A99** (1988) 875

[10] W. Benenson *et al.*, Phys. Rev. Lett. **43** (1979) 683; **44** (1980) 54

[11] E. Chiavassa *et al.*, Nucl. Phys. **A422** (1984)621

[12] Y. Le Bornec *et al.*, Phys. ReV. Lett. **47** (1981) 1870

[13] L. Bimbot *et al.*, Phys. Lett. **114B** (1982)311

[14] A. Anzalone *et al.*, Nucl. Instr. and Meth. **A308** (1991) 533

[15] R. Brun *et al.*, Simulation program for particles physics experiments GEANT - User guide and reference manual. Version 2.00. Data handling division DD/US/86 CERN

[16] S. Kowalski *and* H.A. Enge, "RAYTRACE" February 1, 1986

[17] provided by PHYSICALISCHE NACHWEISGERÄTE, Zimmernerstrasse 9 D 6101 MESSEL (Germany), under the requirements of the CLAMSUD collaboration

[18] see for instance E.P. Lima *et al.* Nucl. Instr. and Meth. **A267** (1988) 93 *and references therein*

[19] Gy. Wolf *et al.*, Phys. ReV. **C43** (1991) R1501

Table captions

Table I - CLAMSUD main characteristics

Table II - Centroids of the intersection point of different trajectories with the central one, obtained for linear momenta from $P = 150\ MeV/c$ to $P = 270\ MeV/c$ with 10 MeV/c steps. In this example $B_0 = 1.7646\ Tesla$. The correlation coefficient of the linear regression for the points from 160 MeV/c up to 240 MeV/c is $r = 0.9993$.

Table III - Investigation on spectrometer characteristics as a function of the displacement of the source (see text). $S.D.$ is the standard deviation of the image on the focal plane projected on the X_F axis; L is the dimension of the focal plane along the X_F direction; the momentum resolution $\delta P/P$ is referred as FWHM.

Table IV - Investigation on spectrometer characteristics as a function of the radial collimation. The symbols have the same meaning as in table III.

Table V - Extension of momentum acceptance to 20%

Table VI - Improvement on $S.D.$ of the particle image on the X_F axis (and consequently on momentum resolution), observing the particle image for 1 cm bins along Z_F axis.

Table VIII Percentage of contaminant muons before and after applying the rejection conditions (see text). P_0 represents the momentum associated to the central trajectory, N_π is the pion number, N_μ the muon number, N_{cond} the number of pions plus the not rejected muons, $N_{\mu res} = N_{cond} - N_\pi$ is the number of non rejected muons (*i.e.* the muons that jet contaminate the spectrum in spite of the rejection conditions). C_{in} and C_{fin} are the muon contaminations without and with software rejection respectively.

TABLE I – CLAMSUD main characteristics.

Maximum central momentum	200 MeV/c
Solid angle	29 msr
Momentum acceptance	$\pm 20\%$
Momentum resolution	$2.6 \cdot 10^{-3}$
Dispersion	1.16 $cm/\%$
Magnification	0.8
Mean trajectory length	1.66 m
Reference gap	8.5 cm
Weight	20 $Tons$
Power	50 $Kwatts$

TABLE II – Example of focal plane calculation.

P	$\langle x \rangle$	$\langle y \rangle$
$[MeV/c]$	$[cm]$	$[cm]$
150	67.99 ± 0.20	27.93 ± 0.50
160	73.76 ± 0.19	28.93 ± 0.43
170	79.53 ± 0.18	30.01 ± 0.37
180	85.34 ± 0.20	31.31 ± 0.38
190	91.05 ± 0.18	32.56 ± 0.32
200	96.75 ± 0.15	33.91 ± 0.27
210	102.45 ± 0.14	35.34 ± 0.25
220	107.94 ± 0.10	36.57 ± 0.17
230	113.29 ± 0.10	37.72 ± 0.17
240	118.39 ± 0.10	38.68 ± 0.17
250	123.43 ± 0.10	39.77 ± 0.18
260	128.46 ± 0.14	41.10 ± 0.25
270	133.39 ± 0.23	42.58 ± 0.41

TABLE III – Effect of source displacement

Δx	P	$\Delta\Omega$	$S.D.$	L	$\delta P/P$
$[cm]$	$[MeV/c]$	$[msr]$	$[mm]$	$[cm]$	$\cdot 10^{-3}$
	170	29.2 ± 1.7	2.8		
0.	200	28.7 ± 1.7	1.8	36.0	3.53
	230	27.8 ± 1.7	2.9		
	170	28.9 ± 1.7	1.7		
1.	200	28.3 ± 1.7	1.4	35.6	2.78
	230	27.0 ± 1.6	1.7		
	170	28.6 ± 1.7	1.5		
2.	200	27.9 ± 1.7	1.3	34.9	2.63
	230	26.5 ± 1.6	1.5		
	170	28.1 ± 1.7	1.3		
3.	200	27.0 ± 1.6	1.3	34.2	2.69
	230	25.7 ± 1.6	1.8		
	170	27.3 ± 1.7	1.4		
4.	200	25.7 ± 1.6	1.6	33.7	3.35
	230	24.3 ± 1.6	2.2		

TABLE IV – Effect of radial collimation

θ_x	P	$\Delta\Omega$	$S.D.$	L	$\delta P/P$
$[mrad]$	$[MeV/c]$	$[msr]$	$[mm]$	$[cm]$	$\cdot 10^{-3}$
	170	28.6 ± 1.7	1.5		
100	200	27.9 ± 1.7	1.3	34.9	2.63
	230	26.5 ± 1.6	1.5		
	170	33.9 ± 1.8	1.9		
120	200	32.9 ± 1.8	1.7	35.0	3.43
	230	31.5 ± 1.7	2.9		
	170	36.2 ± 1.9	2.0		
130	200	35.0 ± 1.9	1.9	35.0	3.83
	230	33.6 ± 1.8	2.6		
	170	43.6 ± 2.1	3.0		
150	200	42.1 ± 2.1	3.1	35.2	6.22
	230	40.6 ± 2.0	4.3		

TABLE V – Effect of ΔP/P = 20%

P	$\Delta\Omega$	$S.D.$	L	$\delta P/P$
$[MeV/c]$	$[msr]$	$[mm]$	$[cm]$	$\cdot 10^{-3}$
160	28.8 ± 1.7	1.6		
170	28.6 ± 1.7	1.5		
200	27.9 ± 1.7	1.3	46.3	2.64
230	26.5 ± 1.6	1.5		
240	26.1 ± 1.6	1.7		

TABLE VI – Improvement in momentum resolution

Z_F [cm]	$S.D.$ [mm]	$\delta P/P$ $\cdot 10^{-3}$
4 ± 0.5	0.93	1.88
2 ± 0.5	0.57	1.15
0 ± 0.5	0.60	1.21
-2 ± 0.5	0.61	1.23
-4 ± 0.5	0.98	1.98
-6 ± 0.5	0.96	1.94

TABLE VII – Drift-chambers main characteristics

Sensitive area	704 x 270 mm^2
Overall dimension of the two chambers	1100 x 560 x 190 mm^3
Number of anode wires	88 per chamber
Spacing between two anode wires	8 mm
Anode-cathode gap	8 mm
Gas volume per chamber	$\sim$ 8 $liters$
Drift time	20 ns/mm
Specific time of cathode delay-line	1.93 ns/mm
Horizontal space resolution	0.3 mm
Vertical space resolution	0.6 mm
Recommended gas-mixture	45% argon, 50% iso-butane, 5% heptane

TABLE VIII – Percentage of contaminant muons

$P_0\ (MeV/c)$	$NTOT$	N_π	N_μ	N_{cond}	$N_{\mu res}$	C_{in}	C_{fin}
50.	1411	1067	344	1082	15	24.4	1.4
67.	4397	3613	784	3699	86	17.8	2.3
90.	11030	9414	1616	9649	235	14.7	2.4
120.	3596	3051	545	3141	94	15.2	3.0

FIGURE CAPTIONS

Fig. 1a - Layout of the CLAMSUD spectrometer. Vertical and horizontal section.

Fig. 1b - The CLAMSUD spectrometer viewed on the median plane. S_0 indicates the source. MW1, MW2, SC1 and SC2 are two multiwire chambers and two sets of plastic scintillators respectively. The master reference system (X_M, Z_M), the source system (X_S, Z_S) and the focal plane system (X_F, Z_F) are also indicated in the figure plane. The Y-axes of the three systems are perpendicular to the median plane and oriented to form with the other axes a clock-wise system.

Fig. 2 - Linear momentum resolution a) and solid angle b) for the central momentum $P = 200\ MeV/c$ as a function of the displacement Δx of the source from an original position (see text).

Fig. 3a - Particle images on the focal plane for three linear momenta P_0, $P_0 \pm 15\%$ (P_0 corresponds to the central trajectory for a given B_0 field).

Fig. 3b - Particle image on the focal plane for the central momentum P_0. The total number of particles hitting the focal plane is 279. The symbol "I" indicates 1 or 2 counts; the symbol "X" indicates more than 2 counts.

Fig. 4 - NIM electronics lay-out

Fig. 5 - $\Delta E - t$ plot, showing the separation between pions and protons for $P = 170\ MeV/c$, $P = 200\ MeV/c$, $P = 230\ MeV/c$.

Fig. 6 - $\Delta E - t$ plot, showing the separation between pions and electrons at $P = 42.5\ MeV/c$, $P = 50\ MeV/c$ and $P = 57.5\ MeV/c$.

Fig. 7 - $\Delta E - t$ plot, showing the separation between pions and electrons for a) $P = 170\ MeV/c$, b) $P = 200\ MeV/c$ and c) $P = 230\ MeV/c$.

Fig. 8 - $\Delta E - t$ plot for protons coming directly from the source (energies of 20, 50, 100, 200, 400 and 600 MeV) and pions selected by the $B\rho$ of the dipole (from 50 up to 200 MeV/c)

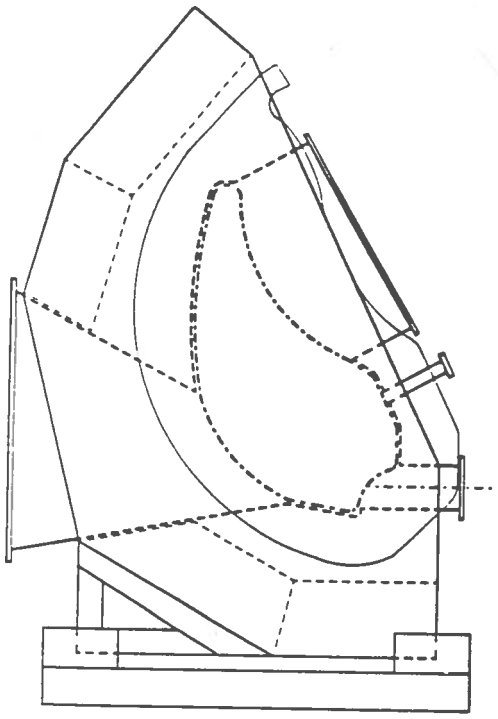

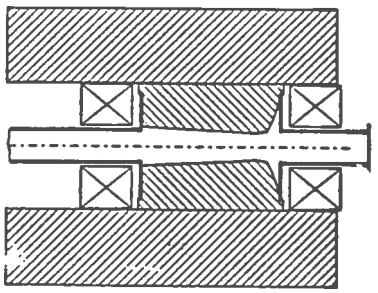

FIG. 1a

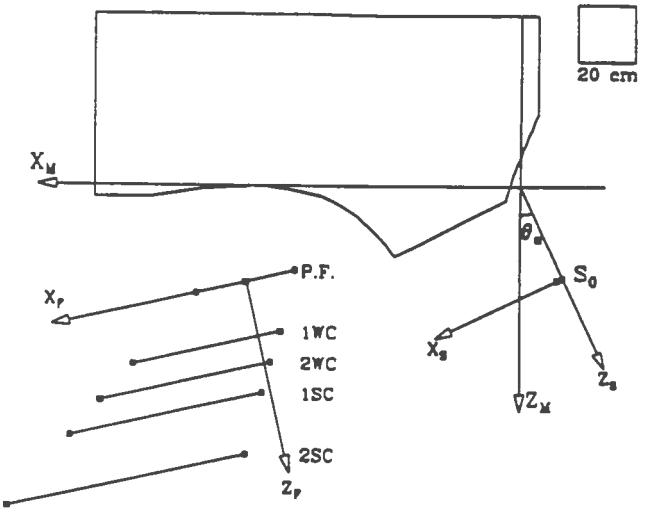

FIG. 1b

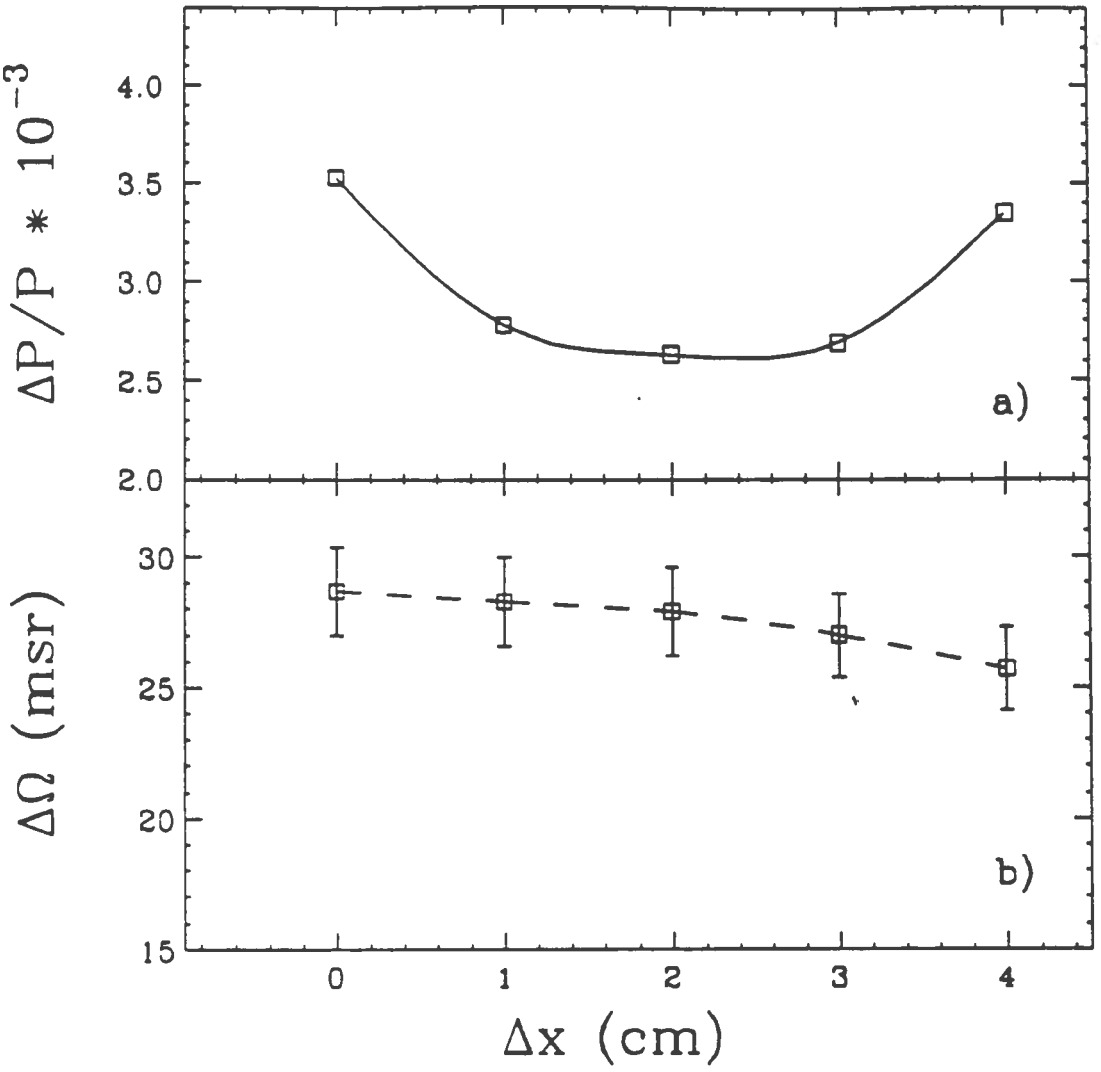

FIG. 2

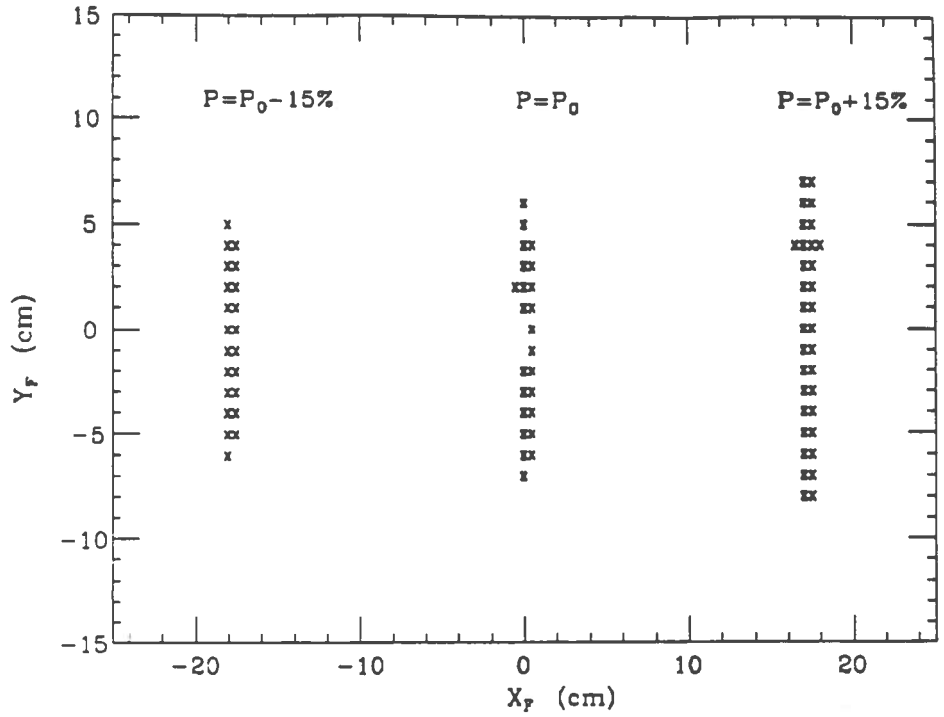
P=P0-15%
P=P0
P=P0+15%
15
10
5
0
-5
-10
-15
-20
-10
0
10
20
YF (cm)
XF (cm)

FIG. 3a

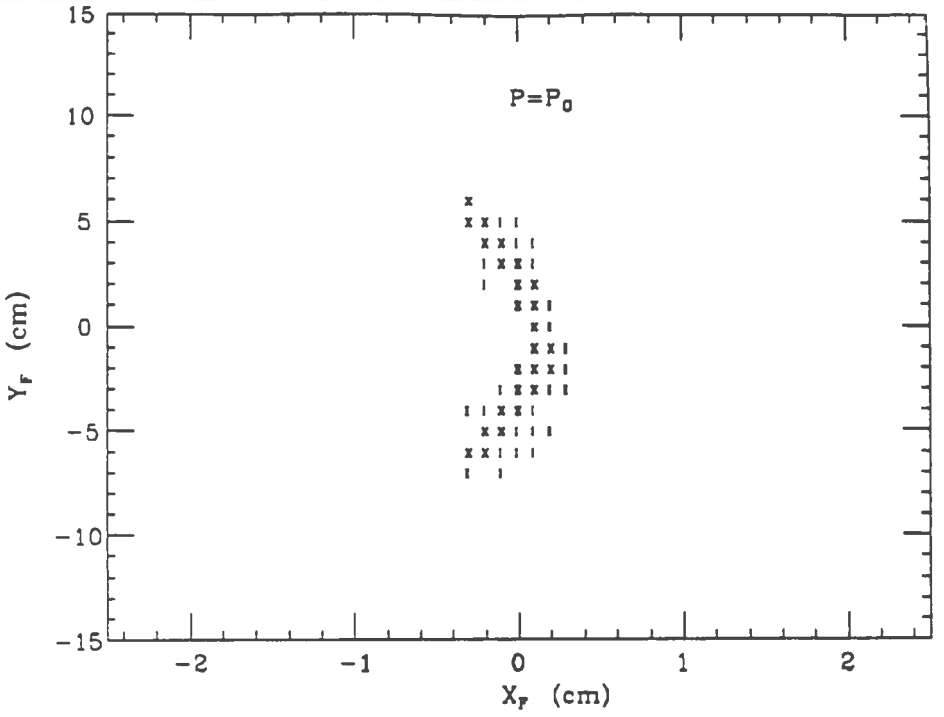
P=P0
15
10
5
0
-5
-10
-15
-2
-1
0
1
2
YF (cm)
XF (cm)

FIG. 3b

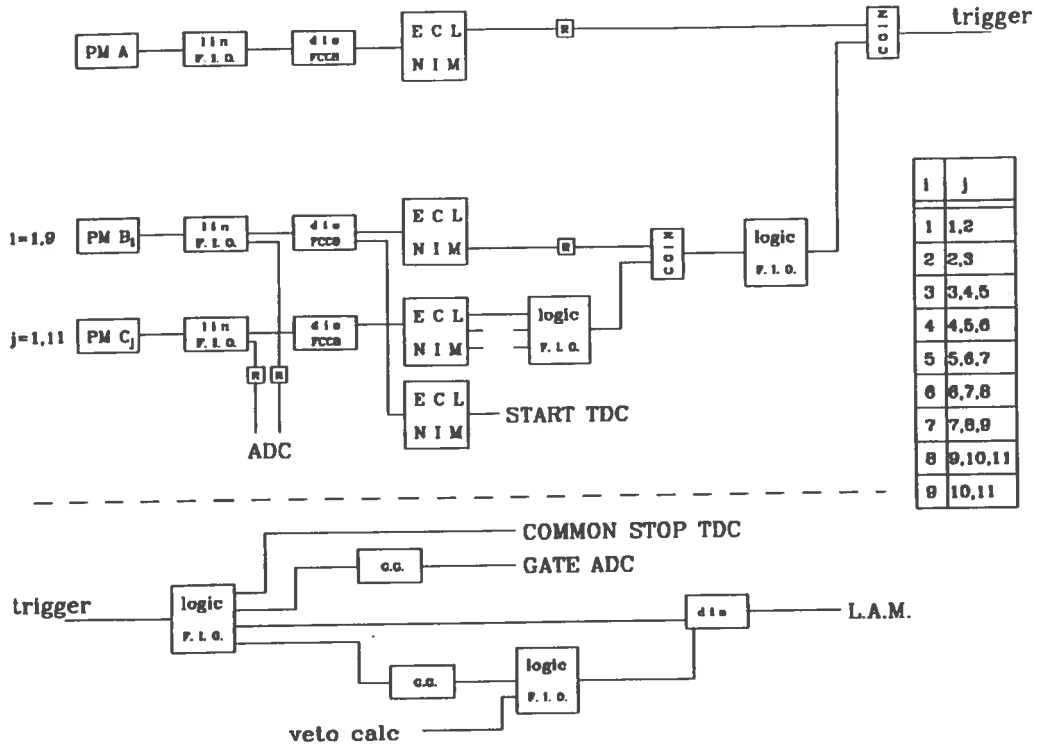
PM A
E C L
N I M
trigger
i=1,9
PM B$_i$
j=1,11
PM C$_j$
logic
ADC
START TDC
COMMON STOP TDC
GATE ADC
trigger
logic
L.A.M.
veto calc
i | j
1 | 1,2
2 | 2,3
3 | 3,4,5
4 | 4,5,6
5 | 5,6,7
6 | 6,7,8
7 | 7,8,9
8 | 9,10,11
9 | 10,11

FIG. 4

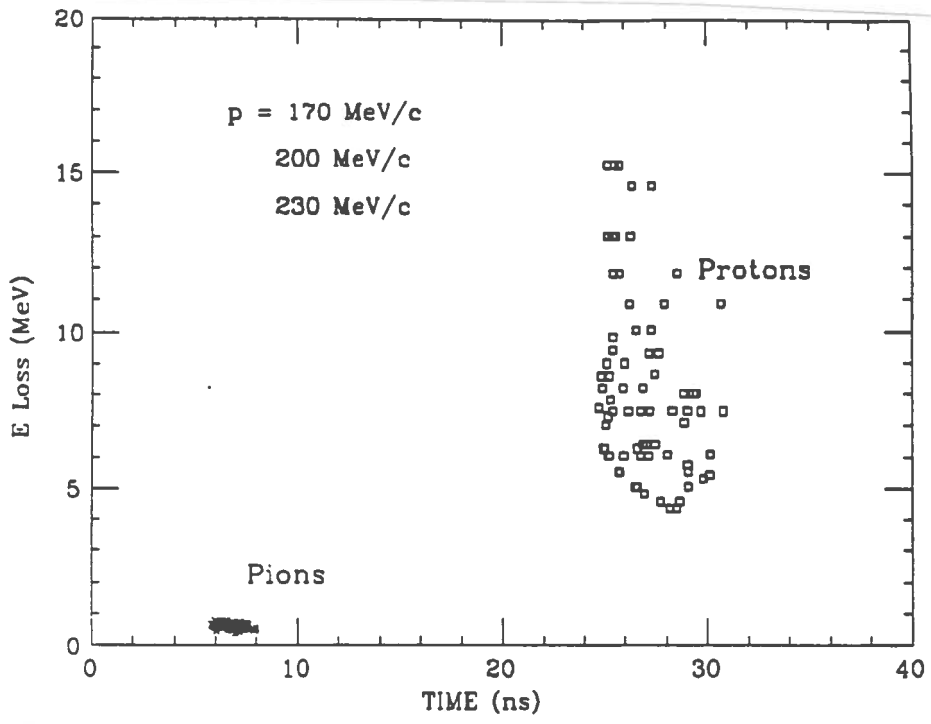
p = 170 MeV/c
200 MeV/c
230 MeV/c
Protons
Pions
E Loss (MeV)
TIME (ns)
0
5
10
15
20
0
10
20
30
40

FIG. 5

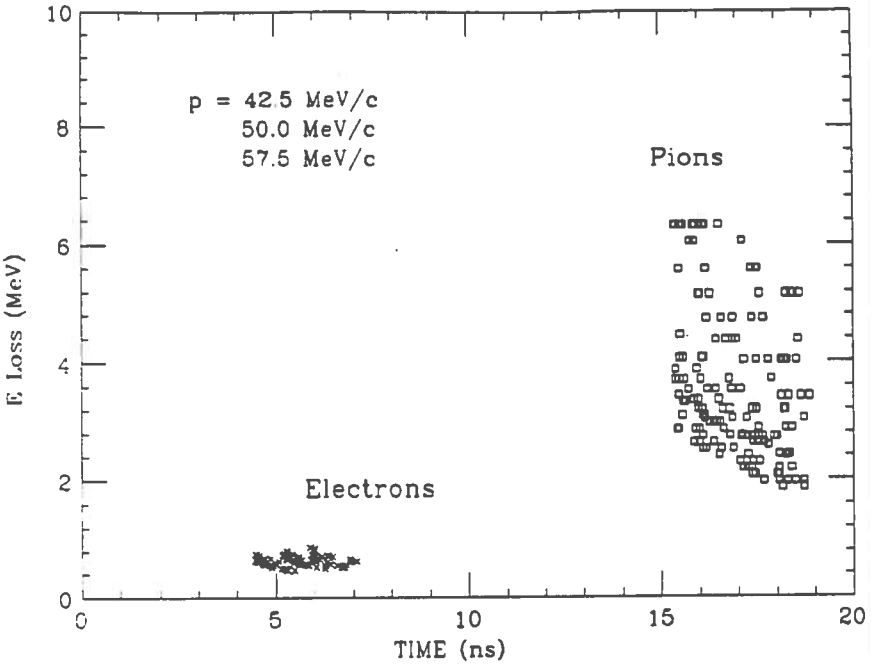
p = 42.5 MeV/c
50.0 MeV/c
57.5 MeV/c
Pions
Electrons
E Loss (MeV)
TIME (ns)

FIG. 6

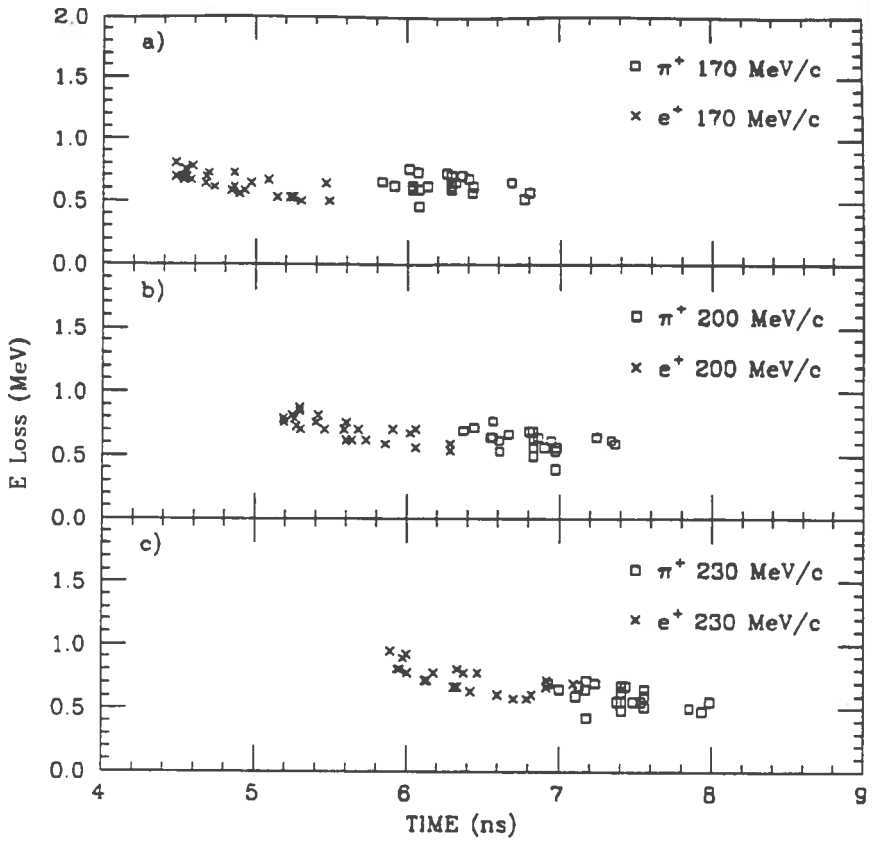
a)
b)
c)
π+ 170 MeV/c
e+ 170 MeV/c
π+ 200 MeV/c
e+ 200 MeV/c
π+ 230 MeV/c
e+ 230 MeV/c
E Loss (MeV)
TIME (ns)

FIG. 7

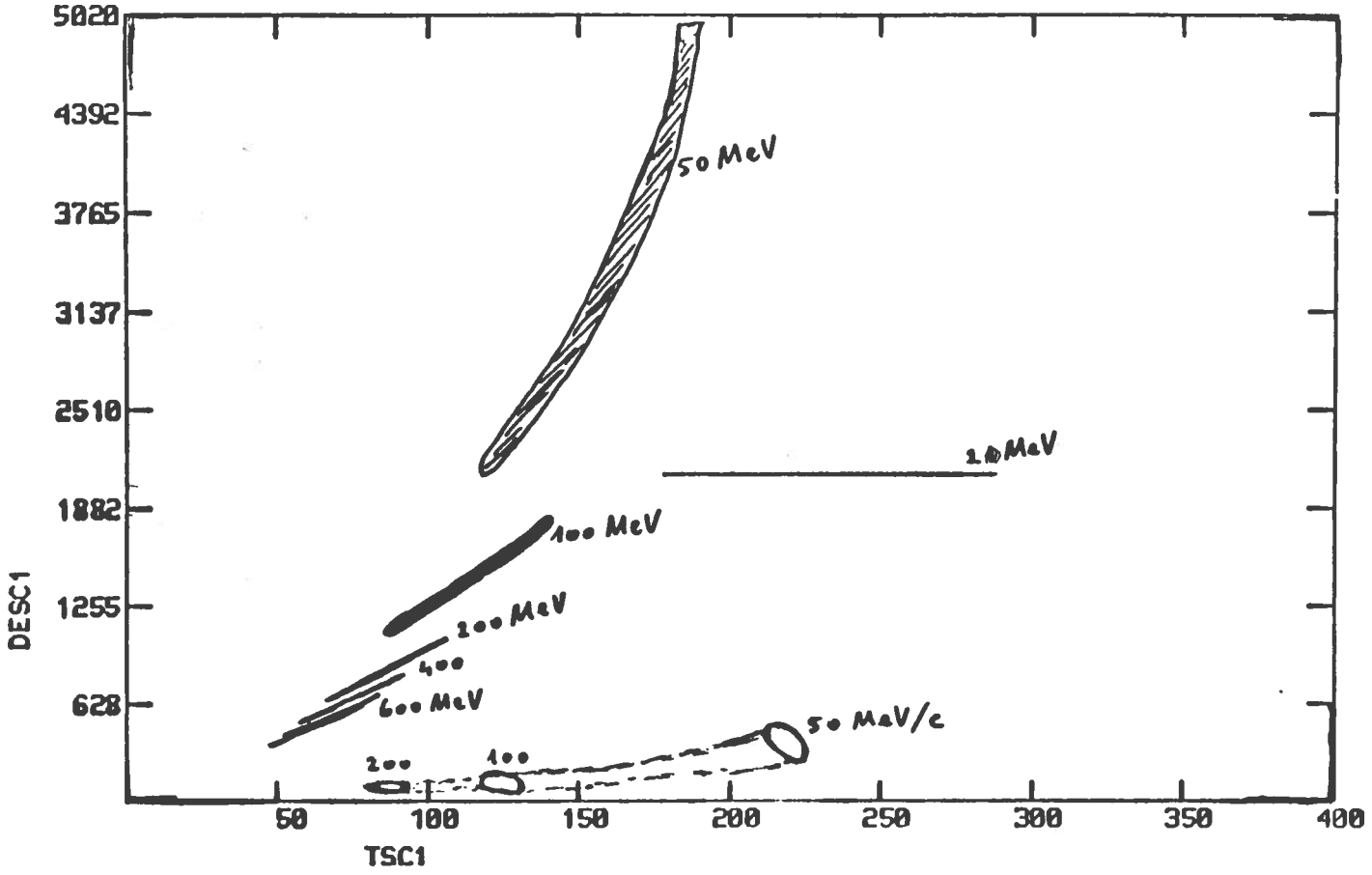
5020
4392
3765
3137
2510
1882
1255
628
DESC1
50 MeV
100 MeV
200 MeV
400
600 MeV
200
400
50 MeV/c
50
100
150
200
250
300
350
400
TSC1

FIG. 8

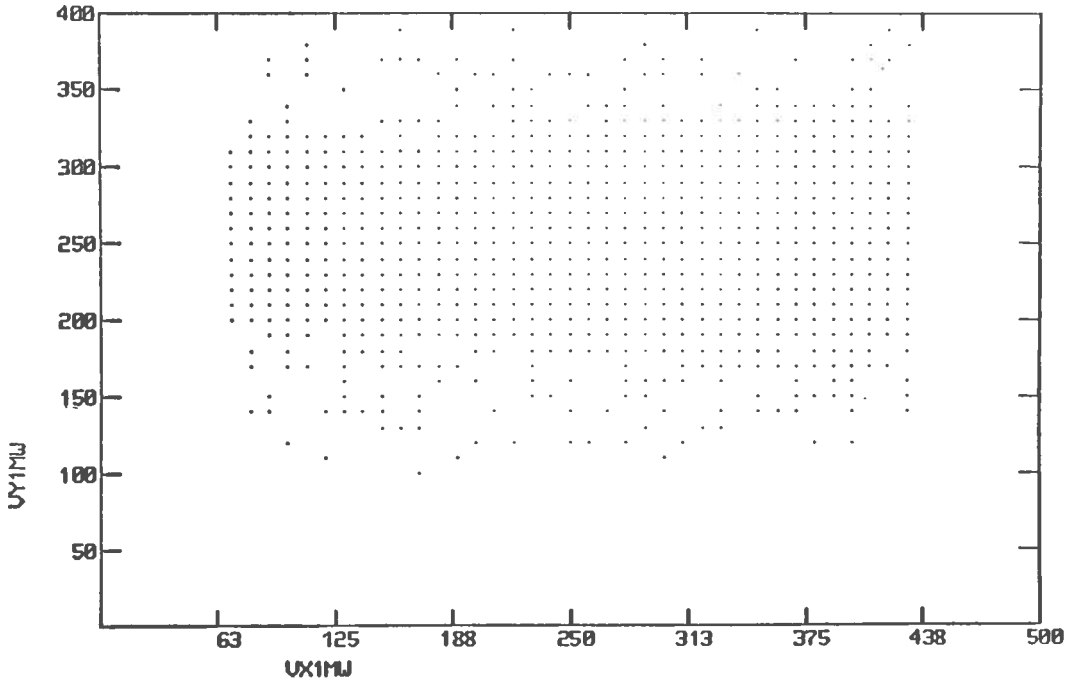
400
350
300
250
200
150
100
50
VY1MW
63
125
188
250
313
375
438
500
VX1MW

FIG. 9a

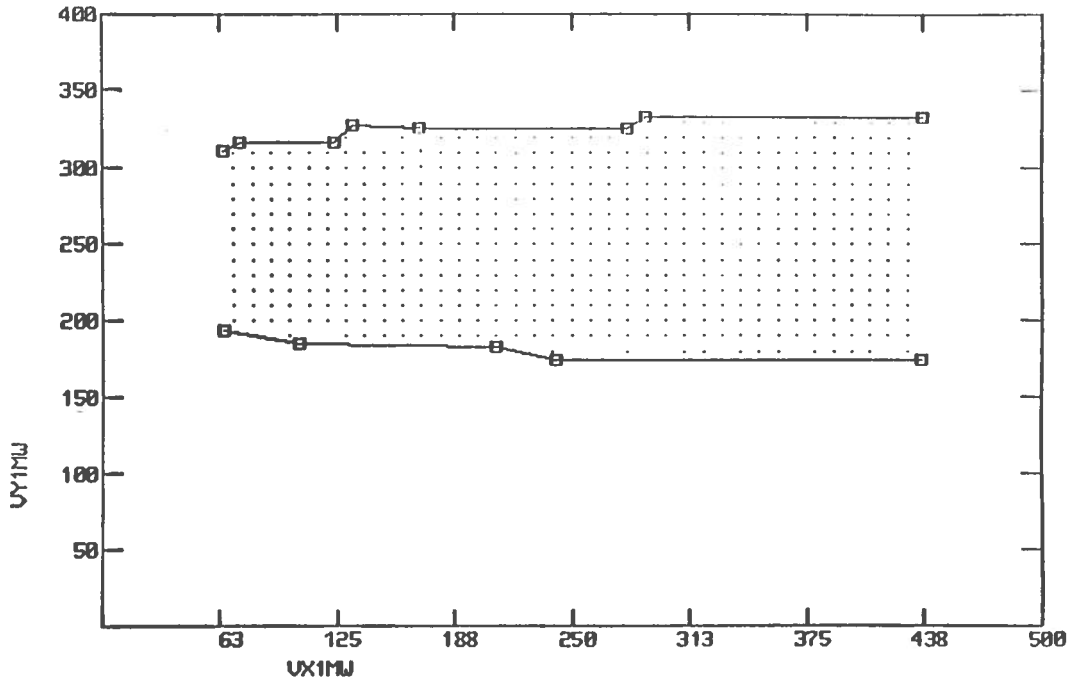
400
350
300
250
200
150
100
50
VY1MW
63
125
188
250
313
375
438
500
VX1MW

FIG. 9b

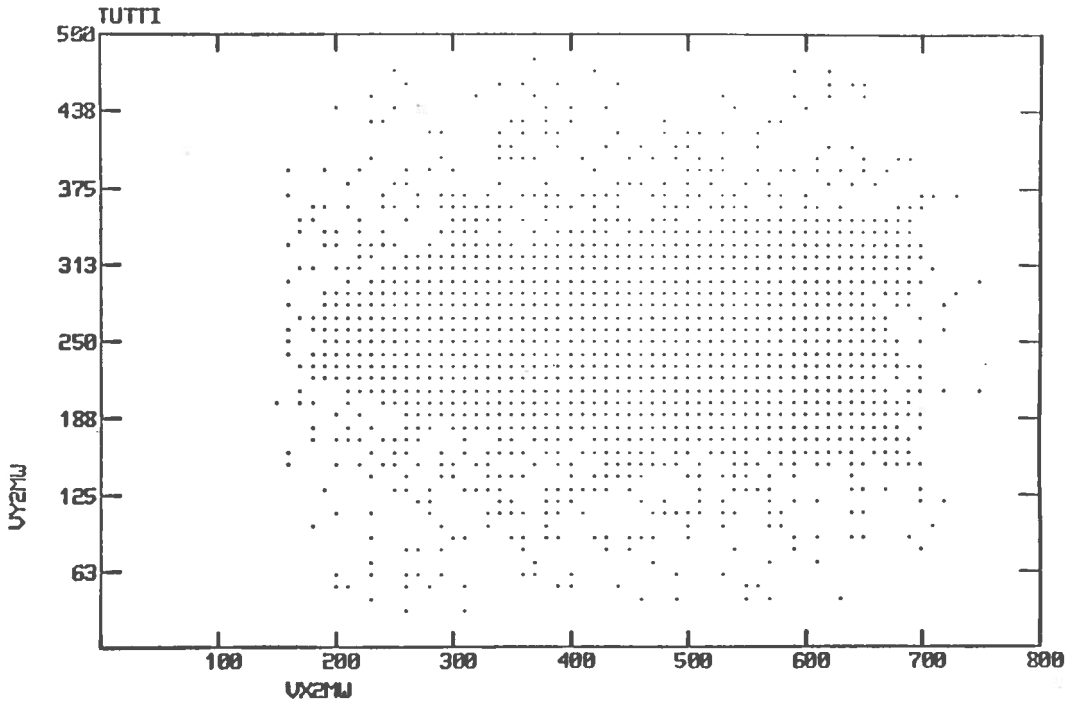

FIG. 10a

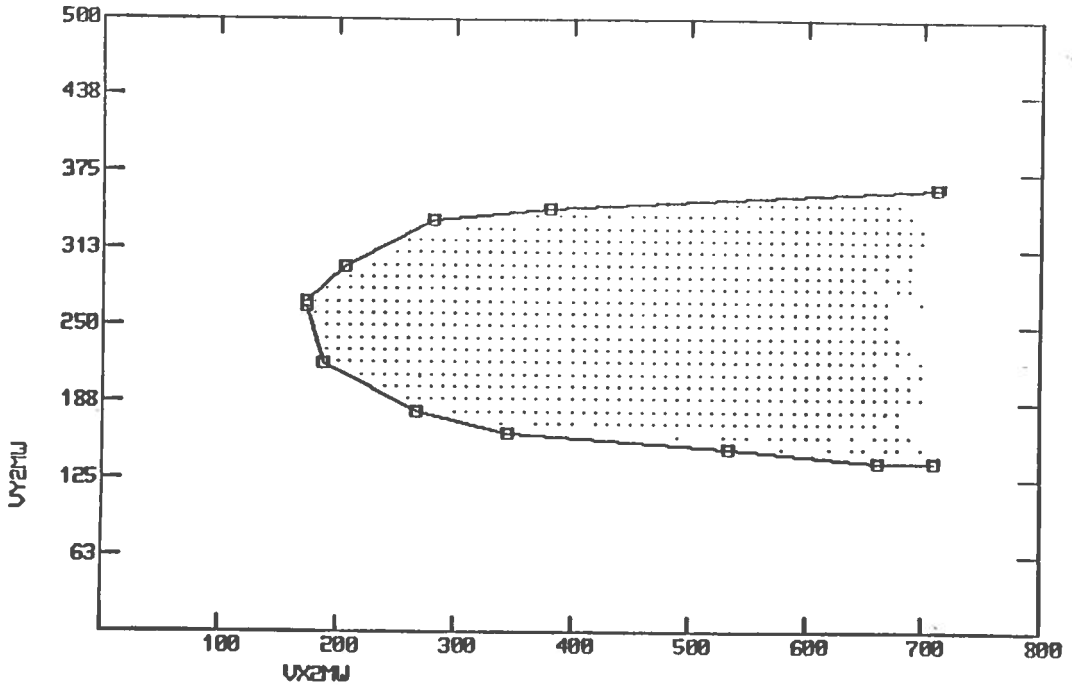

FIG. 10b

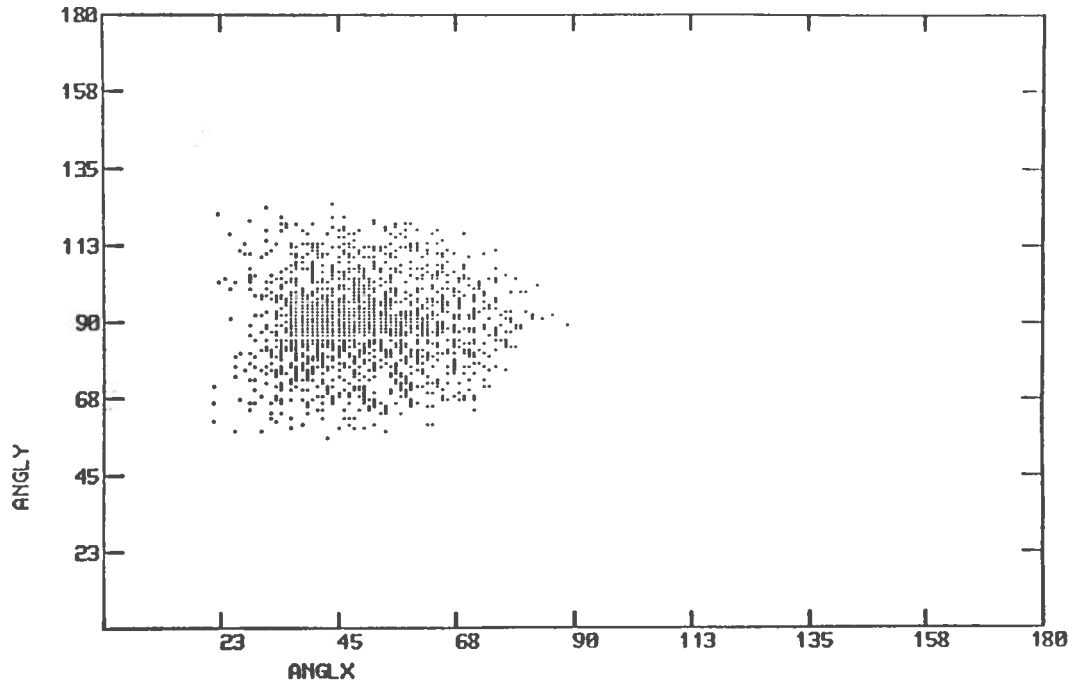

FIG. 11a

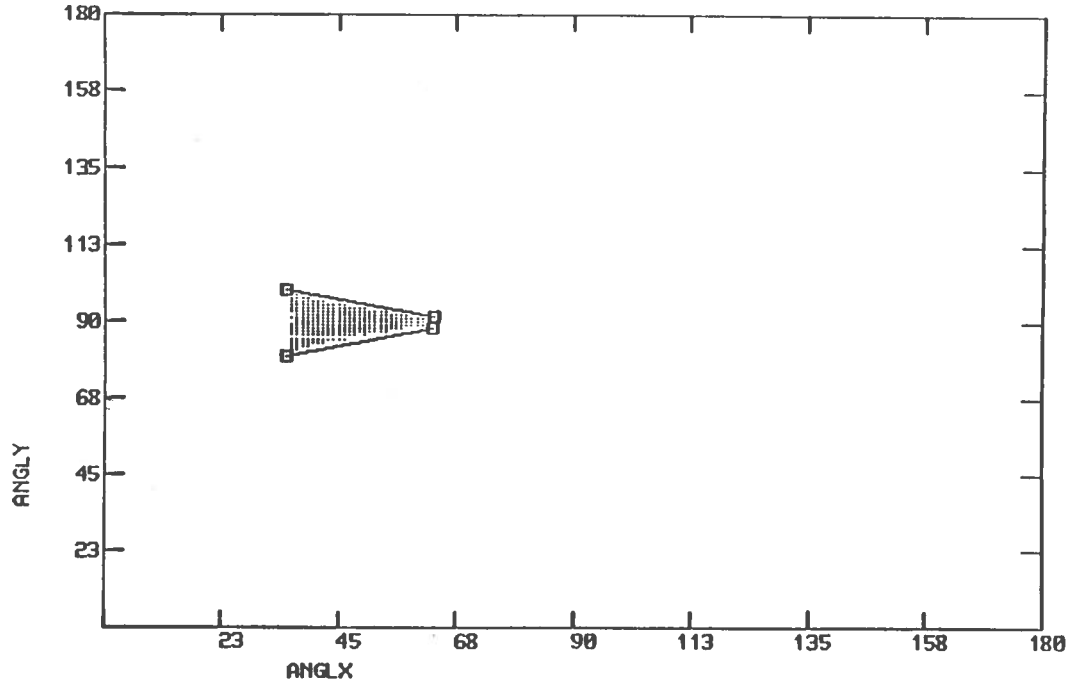

FIG. 11b

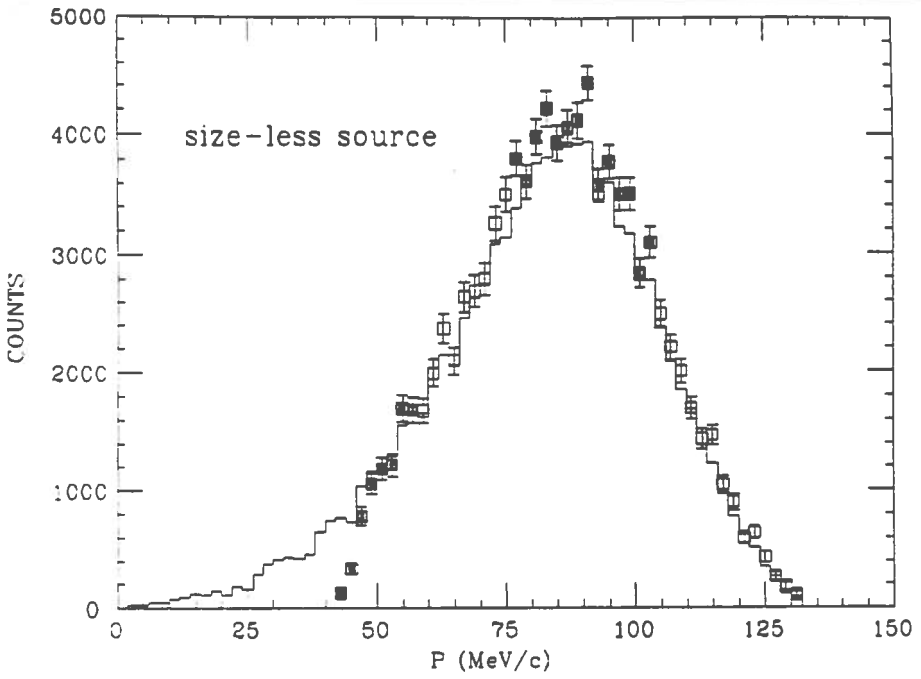
size-less source
COUNTS
P (MeV/c)
0
1000
2000
3000
4000
5000
0
25
50
75
100
125
150

FIG. 12

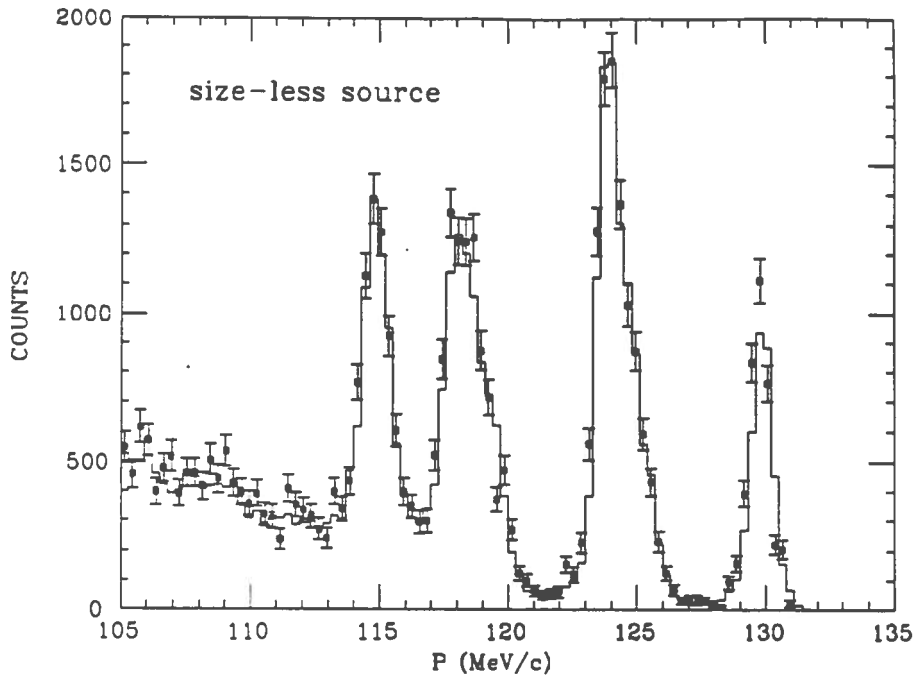
size-less source
COUNTS
P (MeV/c)
0
500
1000
1500
2000
105
110
115
120
125
130
135

FIG. 13

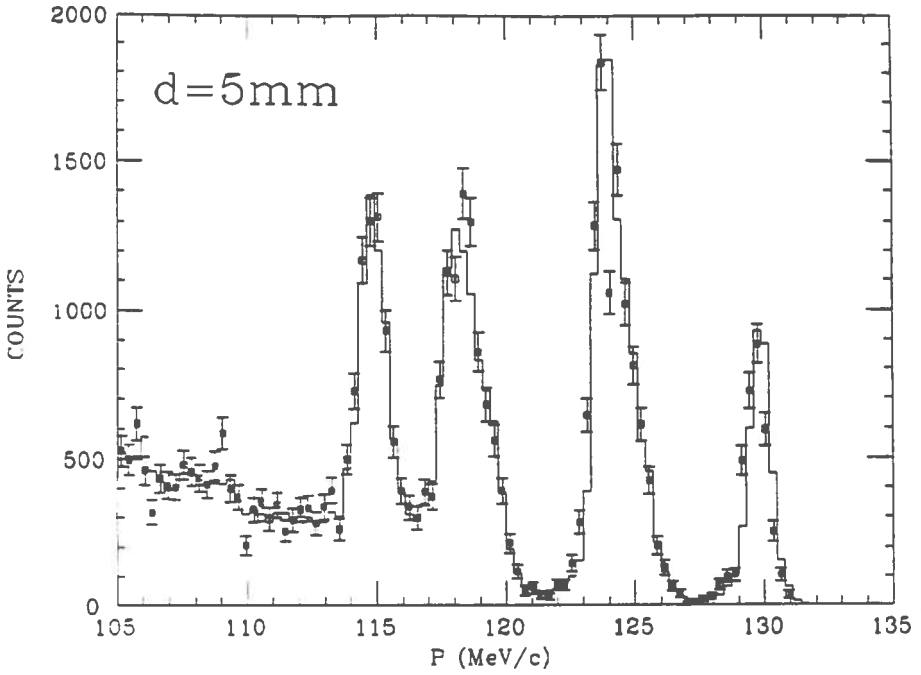

FIG. 14a

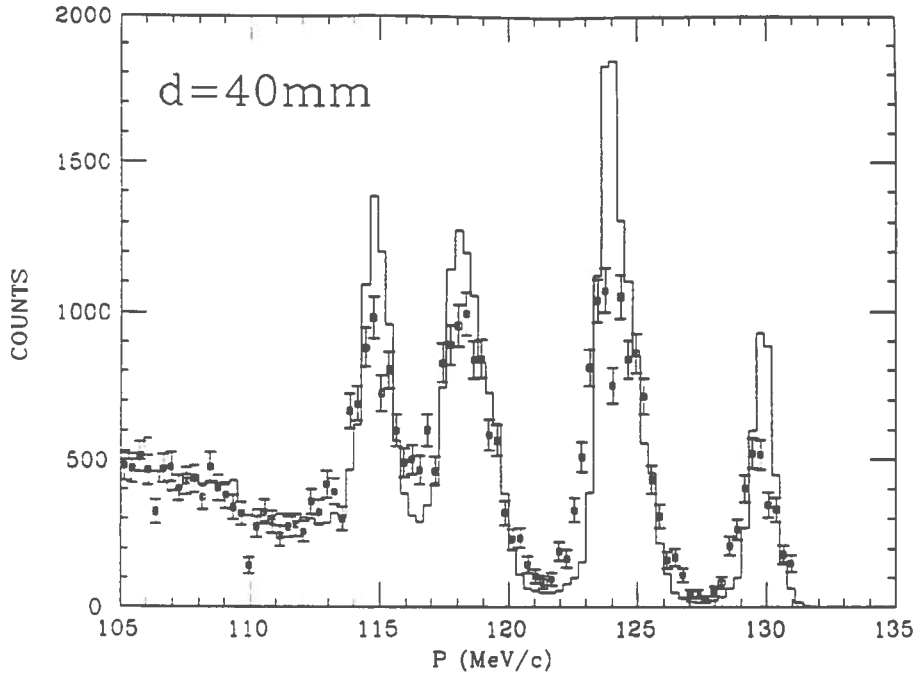

FIG. 14b

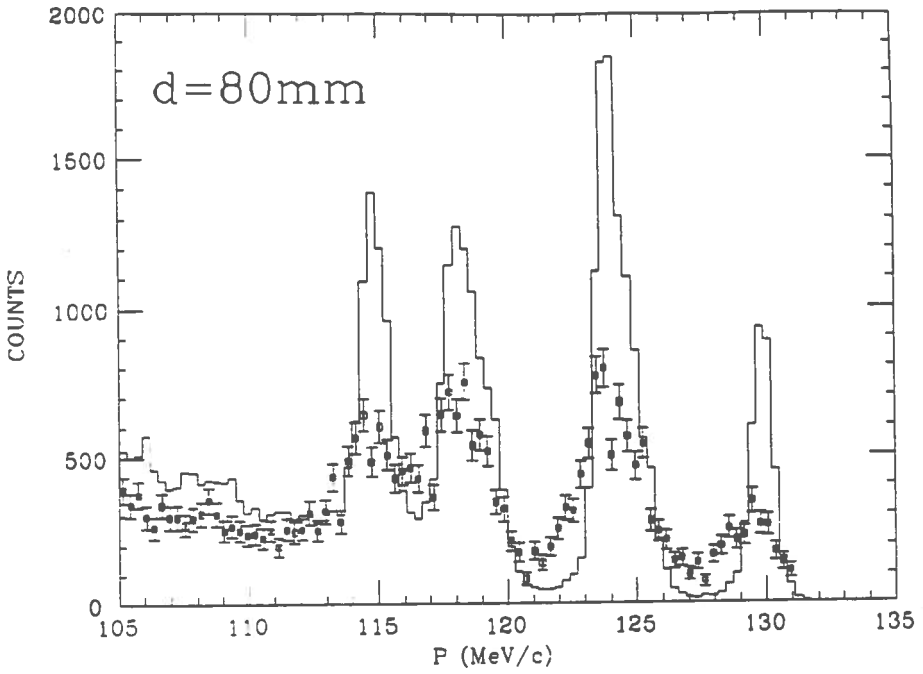

FIG. 14c

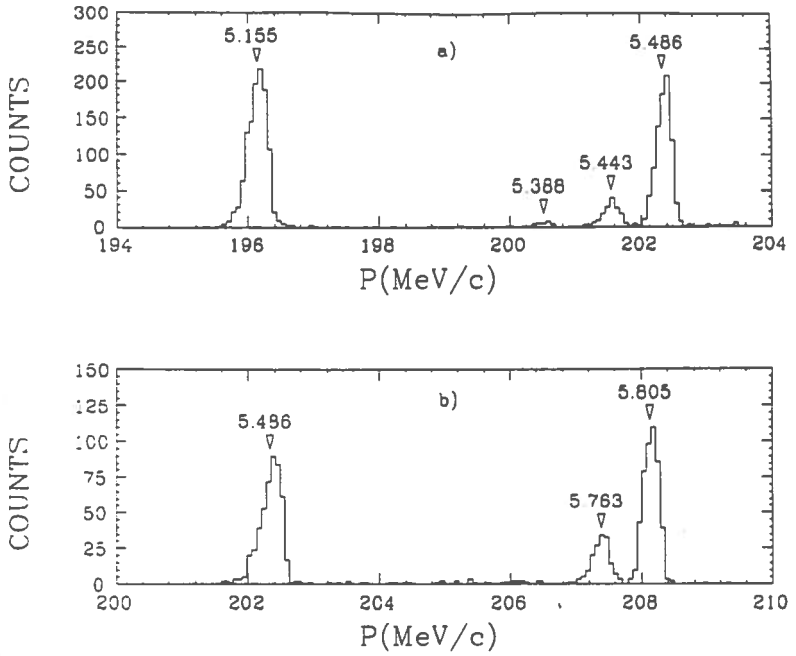

FIG. 15